Optics Letters

Simultaneous excitatory and inhibitory dynamics in an excitable laser

Philip Y. Ma,* Bhavin J. Shastri, Thomas Ferreira de Lima, Chaoran Huang, Alexander N. Tait, Mitchell A. Nahmias, Hsuan-Tung Peng, and Paul R. Prucnal

Department of Electrical Engineering, Princeton University, Princeton, New Jersey 08544, USA
**Corresponding author: yechim@princeton.edu*

Received 19 June 2018; revised 10 July 2018; accepted 11 July 2018; posted 12 July 2018 (Doc. ID 335578); published 1 August 2018

Neocortical systems encode information in electrochemical spike timings, not just mean firing rates. Learning and memory in networks of spiking neurons is achieved by the precise timing of action potentials that induces synaptic strengthening (with excitation) or weakening (with inhibition). Inhibition should be incorporated into brain-inspired spike processing in the optical domain to enhance its information-processing capability. We demonstrate the simultaneous excitatory and inhibitory dynamics in an excitable (i.e., a pulsed) laser neuron, both numerically and experimentally. We investigate the bias strength effect, inhibitory strength effect, and excitatory and inhibitory input timing effect, based on the simulation platform of an integrated graphene excitable laser. We further corroborate these analyses with proof-of-principle experiments utilizing a fiber-based graphene excitable laser, where we introduce inhibition by directly modulating the gain of the laser. This technology may potentially open novel spike-processing functionality for future neuromorphic photonic systems.

OCIS codes: (070.4340) Nonlinear optical signal processing; (200.4700) Optical neural systems.

https://doi.org/10.1364/OL.43.003802

Spiking is a hybrid information-processing technique that combines both the bandwidth efficiency of analog processing and noise robustness of digital computation [1]. It is recognized by the neuroscience community as a sparse coding strategy that widely exists in neural systems for neuromorphic (i.e., brain-inspired) systems [2,3], and it has motivated the recent bloom in spike information processing [4–7]. In the optical domain, spike processing exploits the high speed, high bandwidth, and low crosstalk available to photonic interconnects, aiming to support both computation and communication on a unified platform [8–11]. Photonic spike processing also promises advantages in efficiency, correctness, and adaptability over von Neumann architectures for solving certain tasks, such as pattern recognition, decision making, optimization, and learning [12–14]. Lasers operating in the excitable regime, that is, excitable lasers, have been viewed as promising candidates of neuromorphic photonic systems through their strong analogy with biological neurons in terms of the underlying excitability mechanisms [15]. This close correlation has been experimentally demonstrated in an excitable laser using graphene as the saturable absorber (SA), which exhibits novel spike-processing features such as sharp thresholding and temporal integration [16,17].

The role of inhibition in neural circuit function is well established in neuroscience [18,19]. For decades, neural system models implicitly assumed that neurons encode information via firing rate coding, which is easy to implement but difficult to achieve high information throughput [20]. Temporal coding is an alternative spike-based coding scheme that has been demonstrated to be more efficient in transmitting information but that requires very high precision of the order in which neurons fire [21]. Delivering an inhibitory input to a neuron will determine if the neuron fires a spike and, therefore, facilitate the control over the firing order in nervous systems and neuromorphic photonic systems [22,23].

In optics, since power envelopes are used to represent signals, performing inhibition in the optical domain is an inherent challenge. One all-optical solution showed the use of multiple wavelengths to effect opposing perturbations to semiconductor optical amplifiers operating in the cross-gain modulation regime [24]; however, lacking excitability, this device did not produce sharp all-or-none responses. Another theoretical approach used optical phase to control the effective sign of a perturbation on an excitable laser [25]; however, coordinating the relative optical phases of a network of independent lasers presents a practical challenge. Meanwhile, Tait *et al.* [26] proposed using a balanced photodetector (where two ports receive excitatory and inhibitory pulses, respectively) to drive an electrically injected excitable laser. Most recently, Robertson *et al.* [23] reported controllable inhibitory dynamics in a polarization switching vertical-cavity surface-emitting laser.

In this Letter, we demonstrate the simultaneous excitatory and inhibitory dynamics in a two-section (gain-SA) excitable laser as we extend our preliminary work [27]. We first study these dynamics with a circuit model [28] proposed for an integrated graphene excitable laser (GEL) [16,29], given various biasing conditions, inhibitory strengths, and inhibitory input

timings. We then experimentally investigate the underlying spiking mechanism using a proof-of-principle fiber-based GEL [16], where we introduce inhibition by optically modulating the gain section pumping power. We discover that when the excitatory input lags behind the inhibitory input, the spike output is a function of (1) the pump bias relative to the laser's excitability threshold, and (2) the relative strengths and timings of the excitatory and inhibitory inputs. We also find that the inhibitory input has negligible effect on the spike output if it lags the excitatory input by the time it takes the spike energy to be released.

We first study the simultaneous excitatory and inhibitory dynamics based on the laser neuron circuit model of an integrated GEL, which contains an electrically pumped gain medium and graphene sheets as the SA (five to six layers, saturation energy of 10 pJ). Figure 1(a) shows the circuit simulation setup that drives the GEL circuit model, and we use the same material and geometrical parameters as those in Ref. [28] (except for setting the SA region carrier lifetime as 10 ps for graphene). The gain section input i_{in} consists of three components: $i_{in} = i_{excite} - i_{inhibit} + i_{bias}$, where i_{excite} is the excitatory input, $i_{inhibit}$ is the inhibitory input, and i_{bias} is the DC bias current to the gain section. There is no bias current to the SA section. Figure 1(b) demonstrates the input–output relationship of an integrated GEL with only the excitatory input. The DC bias current to the gain section is 15 mA, which is just below the laser threshold. The excitatory input is a spike whose full width at half maximum (FWHM) is 25 ps, and peak power is 139 mW, providing an appropriate triggering energy that is neither too low (that it cannot trigger spike output or can trigger one spike output but takes a long response time) nor too high (that it may trigger more than one spike output). It takes the integrated GEL approximately 70 ps to respond with a spike output, and this is the $t_{response}$ of the laser for this excitatory input.

Figure 2 illustrates the simulation results of simultaneous excitatory and inhibitory dynamics in an integrated GEL. In addition to the same bias and excitation configuration as above, we add a spike-based inhibitory input also with a FWHM of 25 ps and a peak power of 139 mW. On one hand, the excitatory input can build up the gain level (i.e., carrier concentrations) above the excitability threshold, and saturate the SA to transparency to release a spike output. On the other hand, the inhibitory input can deplete the gain level, which increases the excitatory input energy that will be required to reach the excitability threshold. Figures 2(a)–2(b) show the excitatory and inhibitory inputs with five typical temporal

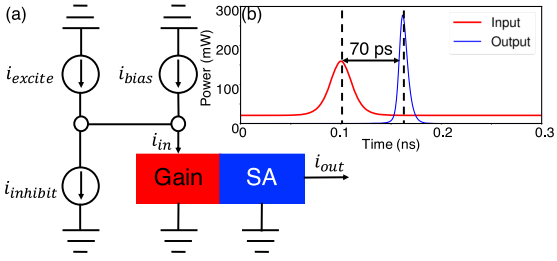

Fig. 1. (a) Circuit simulation setup to simulate the integrated GEL taking both the excitatory and inhibitory inputs. (b) Excitatory dynamics of an integrated GEL with the excitatory input alone (100 mA peak current, 0.72 W/A conversion factor).

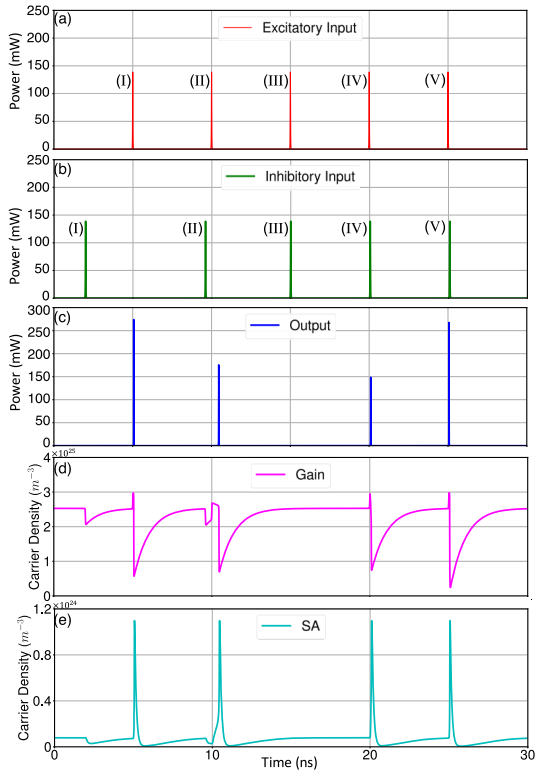

Fig. 2. Simulation results of the (a) excitatory input, (b) inhibitory input, (c) spike output, (d) gain dynamics, and (e) SA dynamics of an integrated GEL. We consider five cases where the excitatory input is lagging the inhibitory input by (I) 4 ns, (II) 400 ps, (III) 0 ps, and is leading by 40 ps and 80 ps for cases (IV) and (V), respectively. In all cases, the bias current is 15 mA; the excitatory and inhibitory inputs have an energy of 4 pJ.

distances. Figures 2(c)–2(e) are the corresponding spike output, gain dynamics, and SA dynamics, respectively. When the excitatory input lags behind the inhibitory input by 4 ns, the gain level has already returned to its equilibrium state as the excitatory input arrives (Case I). Therefore, the integrated GEL behaves as if the inhibitory input did not exist, and it releases a spike output similar to the one in Fig. 1(b). When the excitatory input narrows the time it lags behind the inhibitory input to 400 ps, the gain level cannot return to its equilibrium state the moment the excitatory input arrives (Case II). Although the excitatory input may still raise the gain level above the excitability threshold, the excitatory input energy that can be released by the integrated GEL is reduced, and the spike output is partially suppressed. When the excitatory input and inhibitory input coincide in the temporal domain (Case III), they cancel out each other, and the spike output is completely suppressed. When the excitatory input leads the inhibitory input by only 40 ps (Case IV), the inhibitory input is still within the $t_{response}$ of the laser. In that case, the inhibition will still affect the gain region carrier accumulation and have the spike output partially suppressed. When the excitatory input leads the inhibitory input by 80 ps that is beyond the $t_{response}$ (Case V), the integrated GEL generates the spike output as if there is no inhibitory input.

Figure 3(a) further depicts the simultaneous excitatory and inhibitory dynamics in an integrated GEL with various biasing

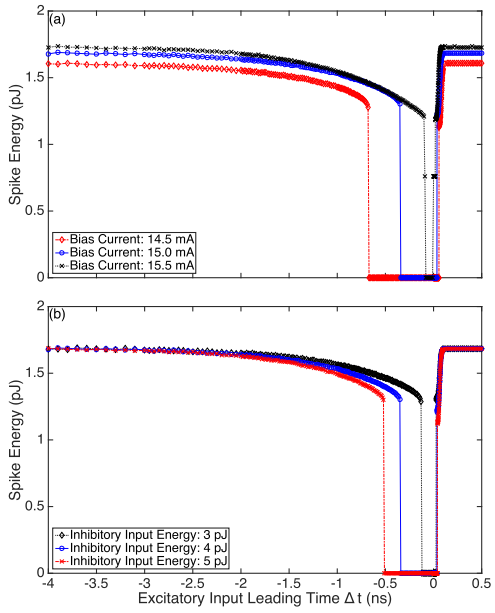

Fig. 3. Simulated spike output energy versus excitatory input leading time with various (a) bias conditions (both excitatory and inhibitory inputs have an energy of 4 pJ), and (b) inhibitory strengths (excitatory input energy: 4 pJ, bias current: 15 mA).

conditions. Here, we define $t_{suppress}$ as the complete suppression range where the output energy is zero. As the bias current is decreased, the effect of the inhibitory pulse on the laser dynamics increases with a $t_{suppress}$ of 118 ps (15.5 mA), 386 ps (15.0 mA), and 737 ps (14.5 mA). Figure 3(b) studies the dynamics in an integrated GEL with various inhibitory strengths. We maintain the same FWHM for the spike-based inhibitory input, but change its power amplitude. As the inhibitory pulse strength is increased relative to the excitatory pulse, $t_{suppress}$ increases from 157 ps (3 pJ) to 386 ps (4 pJ) and 561 ps (5 pJ). While both the biasing condition and inhibitory strength can determine if the spike output will be completely suppressed (and its associated $t_{suppress}$), they do not affect the time it takes the spike output to recover to its normal level when the excitatory input is leading the inhibitory input. The rising edges in Figs. 3(a) and 3(b), both measured to be approximately 70 ps, indicate that the inhibitory input should have negligible effect on the spike output if it lags behind the excitatory input by $t_{response}$.

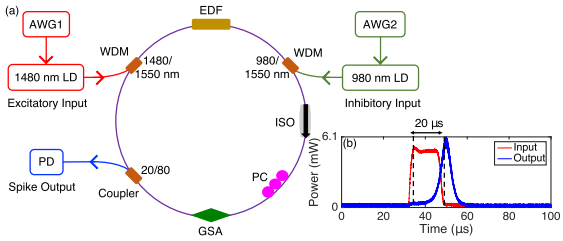

Fig. 4. (a) Experimental setup of the fiber-based GEL is subject to both the excitatory and inhibitory inputs. (b) Excitatory dynamics of a fiber-based GEL with the excitatory input alone.

Next, we demonstrate the feasibility of realizing simultaneous excitatory and inhibitory dynamics in an excitable laser via proof-of-principle experiments using a fiber-based GEL. The experimental setup is shown in Fig. 4(a), where the fiber ring cavity consists of a 75-cm-long gain medium of highly doped erbium-doped fiber (EDF) and a chemically synthesized graphene saturable absorber (GSA), sandwiched between two fiber connectors. The gain and SA sections are separated by an isolator (ISO) to ensure unidirectional propagation and a polarization controller (PC) to enhance output stability. Two arbitrary waveform generators (AWG1 and AWG2) are used to produce excitatory and inhibitory patterns, respectively. AWG1 modulates a 1480 nm laser diode (LD) to generate the excitatory input, while AWG2 modulates a 980 nm LD to generate the inhibitory input. There is no additional pumping signal to the EDF. The high level of the inhibitory pattern provides a standard bias to the laser in a similar way as i_{bias} in the simulation. The low level of the inhibitory pattern lowers the pump power to the gain, which is equivalent to providing an inhibitory input to negate the excitatory input. A 1480/1550 nm wavelength division multiplexer (WDM) and a 980/1550 nm WDM are used to guide the excitatory and inhibitory inputs to the EDF, respectively. The spike output at 1560 nm is coupled out of the system through the 20/80 coupler to a photodiode (PD). Figure 4(b) shows the input–output relationship of the fiber-based GEL (biased at 61 mA) with a single excitatory input pulse. Here, the 1480 nm LD produces an excitatory input whose width is 15 μs and power is 5 mW, while the 980 nm LD offers a constant pumping power to the EDF if biased at 61 mA. The fiber-based GEL responds with a spike output $t_{response} = 20$ μs after the excitatory input.

Figure 5 illustrates the experimental results of simultaneous excitatory and inhibitory dynamics in a fiber-based GEL, which consists of five typical input cases. Here, AWG2 modulates the 980 nm LD to output a 15 μs inhibitory pattern whose high level is 4.4 mW and low level is 0.4 mW. As the inhibitory input moves toward the excitatory input from Figs. 5(a)–5(c), the spike output is gradually suppressed to null.

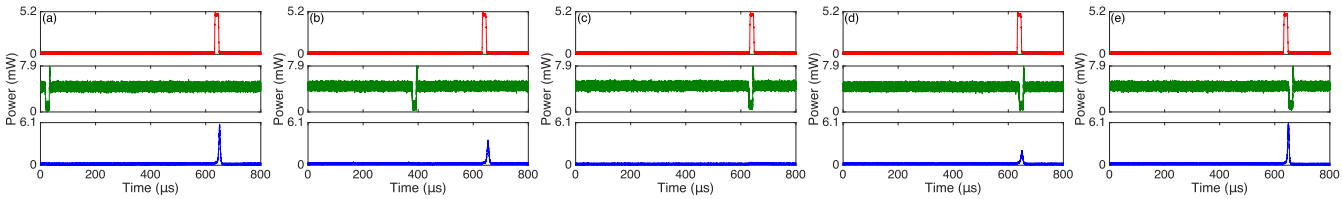

Fig. 5. Experimental waveforms of excitatory input (top), inhibitory input (middle), and spike output (bottom). The excitatory input is lagging the inhibitory input by (a) 611 μs, (b) 250 μs, (c) 0 μs, and it is leading by 11.1 μs and 19.4 μs for cases (d) and (e), respectively. In all cases, the 980 nm LD is biased at 61 mA; the excitatory input energy is 75 nJ, while the (nominal) inhibitory input energy (energy reduction within the inhibitory pattern) is 60 nJ.

As the inhibitory input moves away from the excitatory input from Figs. 5(c)–5(e), the spike output experiences a fast recovery. It can be found that the fiber-based GEL demonstrates similar simultaneous excitatory and inhibitory dynamics as those of the integrated GEL, but at a much slower time scale. This is because the gain region volume of the fiber-based GEL (~cm^3) is much larger than that of the integrated GEL (~μm^3), and the carrier lifetime of the fiber-based GEL (~ms) is much slower than that of the integrated GEL (~ns). Therefore, the rate equations of the fiber-based GEL in our experiments are much slower than those of the integrated GEL.

Figure 6 further characterizes the dynamics in the fiber-based GEL with various biasing conditions [Fig. 6(a)] and inhibitory strengths [Fig. 6(b)]. Similar to simulation results, decreasing the DC bias and increasing the inhibitory strength both contribute to enhancing the suppression of the spike output, creating a $t_{suppress}$ of 60 μs or 100 μs for red curves in these two cases. Furthermore, these experiments share a rising edge of 20 μs, validating the fact that inhibition plays little role in generating the spike output when it lags behind the excitatory input by $t_{response}$. The fact that excitation and inhibition are able to modulate the output strength (especially if inhibition occurs before excitation) enables the excitable laser to serve as a neuromorphic processing node in a large-scale photonic network.

In conclusion, we present the demonstration of simultaneous excitatory and inhibitory dynamics in an excitable laser. We perform numerical analysis based on the simulation platform of an integrated graphene excitable laser that promises an operating speed at ps time scale and a strong compatibility with photonic integrated circuits. We also carry out proof-of-principle experiments using a fiber-based graphene excitable laser, where we propose directly modulating its gain section for inhibition. When the excitatory input is temporally lagging behind the inhibitory input, the spike output suppression effect is closely related to the biasing condition of the laser plus the relative strength and timing difference between the excitatory and inhibitory inputs. When the excitatory input is temporally ahead of the inhibitory input, the spike output suppression is negligible unless the inhibitory input is within the laser's response time. Our approach can potentially contribute to photonic neuromorphic spike processing by bringing novel neural network processing functions into ultrafast computing regimes.

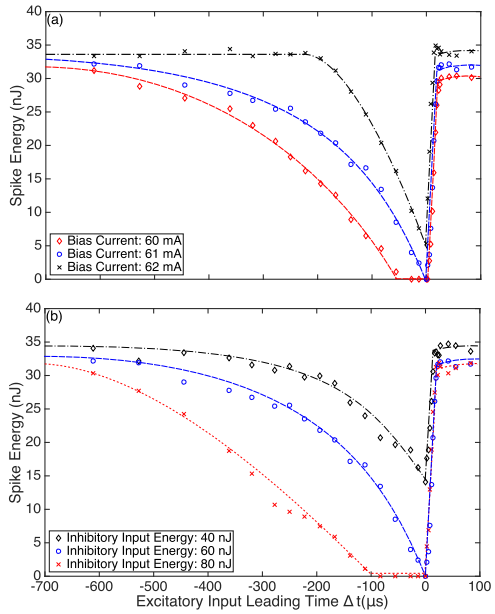

Fig. 6. Experimental spike output energy versus excitatory input leading time with various (a) bias conditions of the 980 nm LD (excitatory input energy, 75 nJ; inhibitory input energy, 60 nJ), (b) inhibitory strengths (excitatory input energy, 75 nJ; bias current for the 980 nm LD, 61 mA).

Funding. National Science Foundation (NSF) (1642962).

REFERENCES

1. R. Sarpeshkar, Neural Comput. **10**, 1601 (1998).
2. A. Borst and F. E. Theunissen, Nat. Neurosci. **2**, 947 (1999).
3. A. Kumar, S. Rotter, and A. Aertsen, Nat. Rev. Neurosci. **11**, 615 (2010).
4. J. Schemmel, D. Briiderle, A. Griibl, M. Hock, K. Meier, and S. Millner, *IEEE International Symposium on Circuits and Systems* (2010), pp. 1947–1950.
5. S. Furber, F. Galluppi, S. Temple, and L. Plana, Proc. IEEE **102**, 652 (2014).
6. B. V. Benjamin, P. Gao, E. McQuinn, S. Choudhary, A. R. Chandrasekaran, J. M. Bussat, R. Alvarez-Icaza, J. V. Arthur, P. A. Merolla, and K. Boahen, Proc. IEEE **102**, 699 (2014).
7. P. A. Merolla, J. V. Arthur, R. Alvarez-Icaza, A. S. Cassidy, J. Sawada, F. Akopyan, B. L. Jackson, N. Imam, C. Guo, Y. Nakamura, B. Brezzo, I. Vo, S. K. Esser, R. Appuswamy, B. Taba, A. Amir, M. D. Flickner, W. P. Risk, R. Manohar, and D. S. Modha, Science **345**, 668 (2014).
8. F. Selmi, R. Braive, G. Beaudoin, I. Sagnes, R. Kuszelewicz, and S. Barbay, Phys. Rev. Lett. **112**, 183902 (2014).
9. A. Aragoneses, S. Perrone, T. Sorrentino, M. C. Torrent, and C. Masoller, Sci. Rep. **4**, 4696 (2014).
10. A. Hurtado and J. Javaloyes, Appl. Phys. Lett. **107**, 241103 (2015).
11. B. Romeira, R. Avo, J. L. Figueiredo, S. Barland, and J. Javaloyes, Sci. Rep. **6**, 19510 (2016).
12. P. R. Prucnal and B. J. Shastri, *Neuromorphic Photonics* (CRC Press, 2017).
13. Y. Shen, N. C. Harris, S. Skirlo, M. Prabhu, T. Baehr-Jones, M. Hochberg, X. Sun, S. Zhao, H. Larochelle, D. Englund, and M. Soljačić, Nat. Photonics **11**, 441 (2017).
14. H. T. Peng, M. A. Nahmias, T. Ferreira de Lima, A. N. Tait, B. J. Shastri, and P. Prucnal, IEEE J. Sel. Top. Quantum Electron. **24**, 6101715 (2018).
15. M. A. Nahmias, B. J. Shastri, A. N. Tait, and P. R. Prucnal, IEEE J. Sel. Top. Quantum Electron. **19**, 1800212 (2013).
16. B. J. Shastri, M. A. Nahmias, A. N. Tait, A. W. Rodriguez, B. Wu, and P. R. Prucnal, Sci. Rep. **6**, 19126 (2016).
17. P. Y. Ma, B. J. Shastri, T. Ferreira de Lima, A. N. Tait, M. A. Nahmias, and P. R. Prucnal, Opt. Express **25**, 33504 (2017).
18. A. R. Aron, Neuroscientist **13**, 214 (2007).
19. S. Ostojic, Nat. Neurosci. **17**, 594 (2014).
20. J. Gautrais and S. Thorpe, Biosystems **48**, 57 (1998).
21. S. Thorpe, A. Delorme, and R. Van Rullen, Neural Netw. **14**, 715 (2001).
22. M. Trevino, Front. Synaptic Neurosci. **8**, 11 (2016).
23. J. Robertson, T. Deng, J. Javaloyes, and A. Hurtado, Opt. Lett. **42**, 1560 (2017).
24. K. Kravtsov, M. P. Fok, D. Rosenbluth, and P. R. Prucnal, Opt. Express **19**, 2133 (2011).
25. K. Alexander, K. Alexander, T. Van Vaerenbergh, M. Fiers, P. Mechet, J. Dambre, and P. Bienstman, Opt. Express **21**, 26182 (2013).
26. A. N. Tait, M. A. Nahmias, B. J. Shastri, and P. R. Prucnal, J. Lightwave Technol. **32**, 4029 (2014).
27. P. Y. Ma, B. J. Shastri, A. N. Tait, M. A. Nahmias, T. Ferreira de Lima, and P. R. Prucnal, in *Conference on Lasers and Electro-Optics (CLEO)*, San Jose, USA, May, 2017, paper SF2 L.6.
28. B. J. Shastri, M. A. Nahmias, A. N. Tait, B. Wu, and P. R. Prucnal, Opt. Express **23**, 8029 (2015).
29. M. A. Nahmias, A. N. Tait, B. J. Shastri, T. Ferreira de Lima, and P. R. Prucnal, Opt. Express **23**, 26800 (2015).